The Journal of Chemical Physics ARTICLE scitation.org/journal/jcp

Slater transition methods for core-level electron binding energies

Cite as: J. Chem. Phys. 158, 094111 (2023); doi: 10.1063/5.0134459
Submitted: 10 November 2022 • Accepted: 16 February 2023 •
Published Online: 6 March 2023

Subrata Jana and John M. Herbert[a)]

AFFILIATIONS

Department of Chemistry and Biochemistry, The Ohio State University, Columbus, Ohio 43210, USA

[a)]Author to whom correspondence should be addressed: herbert@chemistry.ohio-state.edu

ABSTRACT

Methods for computing core-level ionization energies using self-consistent field (SCF) calculations are evaluated and benchmarked. These include a "full core hole" (or "ΔSCF") approach that fully accounts for orbital relaxation upon ionization, but also methods based on Slater's transition concept in which the binding energy is estimated from an orbital energy level that is obtained from a fractional-occupancy SCF calculation. A generalization that uses two different fractional-occupancy SCF calculations is also considered. The best of the Slater-type methods afford mean errors of 0.3–0.4 eV with respect to experiment for a dataset of K-shell ionization energies, a level of accuracy that is competitive with more expensive many-body techniques. An empirical shifting procedure with one adjustable parameter reduces the average error below 0.2 eV. This shifted Slater transition method is a simple and practical way to compute core-level binding energies using only initial-state Kohn–Sham eigenvalues. It requires no more computational effort than ΔSCF and may be especially useful for simulating transient x-ray experiments where core-level spectroscopy is used to probe an excited electronic state, for which the ΔSCF approach requires a tedious state-by-state calculation of the spectrum. As an example, we use Slater-type methods to model x-ray emission spectroscopy.

I. INTRODUCTION

X-ray photoelectron spectroscopy (XPS) is a widely used experimental tool that provides element-specific information for both molecules and solids, but the connection between spectra and structural information is not always straightforward.[1–5] In many cases, theoretical prediction of absolute core-electron binding energies (CEBEs) is needed to resolve experimental ambiguities.[6–14] For this purpose, there are several approaches to compute CEBEs using self-consistent field (SCF) methods, such as density functional theory (DFT).[15–18] Of these, the most widely used procedure is the "ΔSCF" method,[18] in which one explicitly computes a final-state determinant containing a core hole.

The ΔSCF approach has been benchmarked and thoroughly studied for both molecules and solids,[19–24] yet is not without problems. For one, the core hole represents an unstable (saddle-point) solution to the SCF equations and there is no guarantee that such a solution can be located,[25,26] although in our experience this is more of a problem for core excitation than it is for core ionization, meaning that the problem lies with the particle in the virtual space rather than the hole in the occupied space. Sensitivity with respect to the choice of exchange-correlation (XC) functional is an altogether different issue.[27–29] Recent studies have recommended the semilocal SCAN functional[30] for both XPS[21] and x-ray absorption spectroscopy (XAS).[31] The latter technique is not considered here, but for XPS of medium-size molecules, ΔSCF results based on the SCAN functional exhibit mean absolute errors (MAEs) of ~0.2 eV with respect to the experiment.[21] This represents the state-of-the-art in DFT-based ΔSCF calculation of CEBEs.

Whereas the ΔSCF approach includes orbital relaxation via an independent-particle framework, many-body interactions are only included implicitly, via the XC functional. Many-body approaches, such as coupled-cluster theory, incorporate these interactions explicitly and can achieve errors as small as 0.2–0.5 eV for core-level ionization,[32,33] yet these methods are cost-prohibitive except for very small molecules. In addition, the use of a core-hole reference state for the description of dynamical correlation can sometimes lead to singularities because there is a strongly bound orbital in the virtual space.[33–36]

A popular many-body alternative, especially for periodic solids, is the *GW* approach that is based on the single-particle Green's function,[37] for which errors of 0.2–0.5 eV for CEBEs (computed as quasiparticle energies within the *GW* framework) are also typical.[38–40] As with coupled-cluster theory, these calculations are inherently

more expensive than DFT, scaling as $\mathcal{O}(N^6)$ with respect to system size.[41,42] This can be reduced to $\mathcal{O}(N^4)$ with a large prefactor in some recent implementations,[41] but the cost remains much higher than $\mathcal{O}(N^3)$ DFT calculations and is higher still for *GW* calculations that target core states.[38] In addition, *GW* calculations are subject to arbitrary choices that include the choice of representation, leading to apparently unresolvable discrepancies of 0.1–0.2 eV between different implementations.[43,44] More significantly, "*GW*" means not just one but a family of methods with various levels of self-consistency.[45,46] If the *GW* calculations are not fully self-consistent (as is usually the case), then the XC functional that is used to generate the orbitals must be chosen carefully,[47,48] and partially self-consistent approach may not afford continuous potential energy surfaces.[46] (Note that analytic gradients are not available for any of these methods.[42]) Finally, *GW* calculations of core-ionized states are prone to spurious solutions,[39] such that *GW* cannot be considered a black-box method in such cases.[39,40]

For all of these reasons, the ΔSCF approach remains the workhorse tool for the low-cost calculation of CEBEs. Less attention has been paid to methods based on the Kohn–Sham orbital energy levels. These include Koopmans-type approaches based on asymptotically correct XC functionals,[49–51] or alternatively self-interaction-corrected eigenvalues,[52–55] as well as methods based on fractional occupations.[56–63] The latter are the methods considered here. Fractional-occupancy SCF calculations have their historical basis in Slater's transition method (STM).[18,56,57] The formal basis for fractional-electron SCF theory was established later,[64–68] based on an ensemble expression for the chemical potential of an open quantum system. Within DFT, fractional-electron approaches are connected to problems at the heart of modern functional development: self-interaction, delocalization error, and derivative discontinuity.[49,59,67–72] Fractional-electron methods have also been used in the context of correlated wave functions.[73–75]

The STM approach and its subsequent generalizations[58–60] compute electron binding energies directly from Kohn–Sham orbital eigenvalues. Because these one-particle energy levels can directly measure chemical shifts, these methods may hold some advantages for modeling complex systems or experiments, including transient spectroscopy at x-ray or extreme ultraviolet wavelengths.[76–81] To model a pump-probe experiment with the ΔSCF approach, where (for example) an optical pump pulse first prepares a valence excited state, which is subsequently interrogated using an x-ray probe, one would need to construct a core-hole within a ΔSCF calculation of the optically excited state. In our experience,[26] ΔSCF calculations for valence excited states are rather fragile, and this composite calculation runs a significant risk of variational collapse to the ground state.

The aim of this work is to benchmark Slater-type approaches for core-level XPS. With the introduction of one functional-specific parameter, we find that an empirically shifted STM provides accuracy that is competitive with contemporary many-body methods. Because this method connects CEBEs directly to one-particle energy levels, it may provide direct chemical insight into the nature of chemical shifts, e.g., in time-resolved XPS experiments.[81] As an example of more complicated spectroscopy, we apply this method to compute valence-to-core (VtC) emission for a benchmark set of small molecules.

II. THEORY

We begin with a brief review of the ΔSCF method (Sec. II A) before introducing Slater's method (Sec. II B) and its generalizations (Sec. II C).

A. ΔSCF approach

Within the ΔSCF method, the electron binding energy (BE) obtained by ionizing the ith molecular orbital is

$$\mathrm{BE}_i = E_i^{\mathrm{final}}(N-1) - E_0^{\mathrm{initial}}(N), \tag{1}$$

where $E_0^{\mathrm{initial}}(N)$ is the energy of the initial N-electron state and $E_i^{\mathrm{final}}(N-1)$ is the energy of the ionized state. This expression assumes that one can converge a non-*aufbau* Slater determinant that resembles ionization from the indicated orbital. This often requires some type of specialized convergence algorithm,[25,26,82,83] although core-level ionization is perhaps the simplest and most robust non-*aufbau* case.

B. Original Slater method

Slater's transition state concept[56,57] can be used to compute electron BEs in a manner that relies on molecular orbital (MO) energy levels ε_i rather than a difference of total SCF energies, requiring only a single SCF calculation per BE. As such, we omit N from the notation in Eq. (1) and let E denote the ground-state energy of the initial state. Slater considered this energy to be a continuous function of the MO occupation numbers n_i.[18,56,57] We follow a slightly different formulation,[58] taking $E(q)$ to be a function of a single continuous variable q, equal to the fraction of an electron that is removed from whichever MO is to be ionized. [The index of this MO, corresponding to i in Eq. (1), will be implicit.] The energy required to completely ionize this MO can be expressed as[58]

$$\Delta E = \int_1^0 \frac{\partial E(q)}{\partial q}\, dq. \tag{2}$$

For later convenience, we define the integrand to be

$$F(q) = \partial E(q)/\partial q. \tag{3}$$

The Slater–Janak theorem[84] states that the MO eigenvalues are derivatives of the SCF energy with respect to orbital occupation numbers: $\partial E/\partial n_i = \varepsilon_i$. For the ionized MO, $n_i = 1 - q$ so that

$$F(q) = -\varepsilon_i(q). \tag{4}$$

Inserting this result into Eq. (2), the original STM is obtained using a midpoint approximation for the integral, in which the integrand is evaluated at $q = 1/2$:

$$\Delta E_{\mathrm{STM}} = -\varepsilon_i(1/2). \tag{5}$$

The notation means that the SCF calculation is performed with $n_i = 1/2$, i.e., with half an electron in the MO that is to be ionized. The resulting orbital energy level directly approximates BE_i.

Long ago, Williams *et al.*[58] proposed a slightly different version of Slater's method, based on an alternative quadrature applied to Eq. (2). The resulting expression for BE_i is

$$\Delta E_{\mathrm{STM}'} = -\varepsilon_i(2/3), \tag{6}$$

TABLE I. Definition of various Slater-type approximations for BE_i.

Name	Scheme	n	Leading error	No. SCFs required	Expression for BE_i
STM[a]	$\mathcal{F}[n]$	2	$-\frac{1}{4}E^{(3)}$	1	$-\varepsilon_i(1/2)$
STM[b]	$\mathcal{F}[n]$	3	$\frac{1}{3}E^{(2)}$	1	$-\varepsilon_i(2/3)$
STM	$\mathcal{F}[n]$	4	$\frac{1}{2}E^{(2)}$	1	$-\varepsilon_i(3/4)$
GSTM[c]	$\mathcal{F}[0;n]$	3	$-\frac{1}{9}E^{(4)}$	2	$-\frac{1}{4}[\varepsilon_i(0)+3\varepsilon_i(2/3)]$
GSTM	$\mathcal{F}[0;n]$	4	$\frac{1}{8}E^{(3)}$	2	$-\frac{1}{3}\varepsilon_i(0)-4\varepsilon_i(3/4)$
GSTM[c]	$\mathcal{F}[0;n]+\mathcal{F}[1;n]$	2	$\frac{1}{24}E^{(5)}$	3	$-\frac{1}{6}[\varepsilon_i(0)+\varepsilon_i(1)+4\varepsilon_i(1/2)]$
GSTM[c]	$\mathcal{F}[0;n]+\mathcal{F}[1;n]$	3	$\frac{1}{54}E^{(5)}$	4	$-\frac{1}{8}[\varepsilon_i(0)+\varepsilon_i(1)+3\varepsilon_i(2/3)+3\varepsilon_i(1/3)]$

[a]Original Slater method.[57]
[b]Method of Williams *et al.*[58]
[c]Proposed by Hirao *et al.*[59]

meaning that a different fractional occupancy ($n_i = 2/3$) is used, as compared to Slater's original approach. We will refer to both of these approximations as STMs, and they are collected in Table I along with some other approximations that are introduced below. What Eqs. (5) and (6) share in common is that either method requires only a single (fractional-electron) SCF calculation to estimate BE_i. In contrast, the generalized (G)STM approximations that are introduced below each require two or more SCF calculations. This additional complexity may be warranted if the agreement with ΔSCF improves.

C. Generalized fractional occupation methods

To derive GSTMs, we follow the formalism of Hirao *et al.*[59] and express $E(q)$ as a Taylor series about the point $q = 0$:

$$E(q) = \sum_{k=0}^{\infty} q^k E^{(k)}, \tag{7}$$

where

$$E^{(k)} = \frac{1}{k!}\left(\frac{\partial^k E}{\partial q^k}\right)\bigg|_{q=0}. \tag{8}$$

Limiting values of Eq. (7) are $E(0) = E_0^{\text{initial}}$ at $q = 0$ and

$$E(1) = \sum_{k=0}^{\infty} E^{(k)} = E_i^{\text{final}}, \tag{9}$$

at $q = 1$, where the choice of which MO is to be ionized (index i) is again implicit.

According to this formalism, BE_i is given by

$$\begin{aligned}\Delta E &= E_i^{\text{final}} - E_0^{\text{initial}} \\ &= E^{(1)} + E^{(2)} + E^{(3)} + \cdots.\end{aligned} \tag{10}$$

Differentiation of Eq. (7) affords

$$F(q) = \sum_{k=1}^{\infty} k q^{k-1} E^{(k)}, \tag{11}$$

with limiting values

$$F(0) = E^{(1)} \tag{12}$$

for the original molecule and

$$F(1) = \sum_{k=1}^{\infty} k E^{(k)} \tag{13}$$

for its cation. The procedure followed by Hirao *et al.*[59] is to search for combinations of $F(q) = -\varepsilon_i(q)$ and $F(q') = -\varepsilon_i(q')$, with different fractional occupancies q and q', in order to cancel leading-order errors in the Taylor series that defines ΔE in Eq. (10). The quantities $F(q)$ and $F(q')$ require separate fractional-occupancy SCF calculations.

We will formulate this process in a somewhat different way by rewriting Eq. (11) as a polynomial expansion in $q = 1 - 1/n$, where n is an integer and q represents the fractional charge that is removed from the MO to be ionized. This will define a sequence of approximations $\mathcal{F}[n]$ for $n = 2, 3, \ldots$:

$$\mathcal{F}[n] \equiv F(1 - 1/n) = \sum_{k=1}^{\infty} k(1 - 1/n)^{k-1} E^{(k)}. \tag{14}$$

As indicated in Table I, the $\mathcal{F}[2]$ scheme corresponds to the original STM and $\mathcal{F}[3]$ is the alternative formula derived by Williams *et al.*[58] Error estimates follow when $\mathcal{F}[n]$ is subtracted from ΔE in Eq. (10).

The original STM incurs an error at third order in the expansion of $E(q)$, as indicated in Table I, but judicious combinations of eigenvalues from multiple fractional-occupancy SCF calculations can reduce this error.[59] To examine some of these approximations, we start by defining

$$\mathcal{F}[0;n] = F(0) + nF(1 - 1/n), \tag{15}$$

from which one can obtain

$$\mathcal{F}[0;n] = (n+1)E^{(1)} + \sum_{k=2}^{\infty} kn(1 - 1/n)^{k-1} E^{(k)}. \tag{16}$$

The first few terms are

$$\mathcal{F}[0;n] = (n+1)E^{(1)} + 2n(1-1/n)E^{(2)} + 3n(1-1/n)^2E^{(3)} + 4n(1-1/n)^3E^{(4)} + 5n(1-1/n)^4E^{(5)} + \cdots. \quad (17)$$

The quantities $\mathcal{F}[0;n]$, with different values of n, provide approximations for BE_i. To see how this is so, consider the case $n = 3$. The result for $\mathcal{F}[0;3]$ can be rewritten as

$$\frac{1}{4}[F(0) + 3F(2/3)] = E^{(1)} + E^{(2)} + E^{(3)} + \frac{8}{9}E^{(4)} + \cdots. \quad (18)$$

Subtracting this expression from the ΔSCF result in Eq. (10), one observes a cancellation of the first three terms, leaving

$$\Delta E - \frac{1}{4}[F(0) + 3F(2/3)] = -\frac{1}{9}E^{(4)} + \cdots. \quad (19)$$

Therefore, the evaluation of the quantity on the left side of Eq. (18) incurs an error at fourth order in the expansion of $E(q)$. This is superior to the third-order error incurred by the original STM. By virtue of the Slater–Janak theorem, the corresponding approximation for BE_i is

$$\Delta E_{\mathrm{GSTM}} = -\frac{1}{4}[\varepsilon_i(0) + 3\varepsilon_i(2/3)]. \quad (20)$$

This result was originally derived by Hirao *et al.*[59]

We will call the approximation in Eq. (20) a GSTM because it requires two SCF calculations to obtain BE_i, one with $q = 0$ and another with $q = 2/3$. However, $q = 0$ corresponds to a standard integer-occupancy SCF calculation, which is often a prerequisite for performing fractional-occupancy SCF calculations. In that case, this particular GSTM does not incur additional overhead as compared to the STMs described in Sec. II B. The method of Eq. (20) is listed in Table I under the nomenclature $\mathcal{F}[0;n]$ with $n = 3$. The $n = 4$ result, $\mathcal{F}[0;4]$, is also shown for comparison; however, this approach incurs cubic rather than quartic error in $E(q)$, despite also requiring two SCF calculations.

By analogy to Eq. (15), we next define

$$\mathcal{F}[1;n] = F(1) + nF(1/n) = (n+1)E^{(1)} + \sum_{k=2}^{\infty}[kn(1-1/n)^{k-1} + k]E^{(k)}. \quad (21)$$

By virtue of Eq. (4), this represents the cation eigenvalue $F(1)$ plus a correction based on an SCF calculation with a small fraction of an electron, $q = 1/n$. With $n = 3$, the $\mathcal{F}[1;3]$ scheme also exhibits fourth-order error, analogous to the $\mathcal{F}[0;3]$ scheme.[59]

An alternative is to take the sum

$$\mathcal{F}[0;n] + \mathcal{F}[1;n] = 2(n+1)E^{(1)} + \sum_{k=2}^{\infty}\gamma_k E^{(k)}. \quad (22)$$

Here, $\gamma_k = 2kn(1-1/n)^{k-1} + k$ for $n \geq 2$. With $n = 2$, this formula yields

$$F(0) + 2F(1/2) + F(1) + 2F(1/2) = 6E^{(1)} + 6E^{(2)} + 6E^{(3)} + 6E^{(4)} + \frac{25}{4}E^{(5)} + \cdots. \quad (23)$$

As such, the quantity $(\mathcal{F}[0;2] + \mathcal{F}[1;2])/6$ affords the ΔSCF value of BE_i through $E^{(4)}$, with a leading-order error equal to $-E^{(5)}/24$. A similar exercise for $n = 3$ demonstrates that

$$\frac{1}{8}[F(0) + F(1) + 3F(2/3) + 3F(1/3)] = E^{(1)} + E^{(2)} + E^{(3)} + E^{(4)} + \frac{55}{44}E^{(5)} + \cdots. \quad (24)$$

These two schemes, each with fifth-order error, are also listed in Table I. The one with $n = 3$ has a smaller formal error but requires four separate SCF calculations, whereas the method with $n = 2$ requires only three separate SCF calculations, and only one of those with fractional occupation numbers.

III. COMPUTATIONAL DETAILS

We will test some of the STM and GSTM approaches using the "CORE65" dataset,[39] which consists of 65 experimental K-shell CEBEs for the elements carbon (30 CEBEs in the dataset), oxygen (21 CEBEs), nitrogen (11 CEBEs), and fluorine (3 CEBEs). Various density functional approximations are tested, including the SCAN functional[30] along with its hybrid SCAN0,[85] the latter of which includes 25% Hartree–Fock exchange (HFX); the B3LYP functional;[86,87] Becke's "half-and-half" functional (BH&HLYP), which contains 50% HFX; the range-separated hybrid functional ωB97X-V;[88] and two long-range corrected (LRC) functionals,[89] namely, LRC-ωPBE and LRC-ωPBEh,[90,91] the latter of which includes 20% HFX at short range. We also examine the short-range corrected (SRC) functional SRC1-r1,[92] which was parameterized for XAS at the K-edge of "first row" elements (meaning C, O, N, and F) and contains 50% HFX on a length scale of <1 Å.[92,93] Range separation parameters for the two LRC functionals were set to $\omega = 0.3$ bohr^{-1} (LRC-ωPBE) and $\omega = 0.2$ bohr^{-1} (LRC-ωPBEh), which are the statistically optimized values for a dataset that includes both thermochemistry and excitation energies.[90,94,95]

The def2-QZVP basis set is used for all production calculations. It has been suggested that additional core functions are required for CEBE calculations, in order to describe orbital relaxation associated with the core hole,[63,96,97] but we find that def2-QZVP is sufficiently close to the basis-set limit as to make this unnecessary. For ΔSCF methods, a completely uncontracted version of def2-QZVP, which should better describe core-hole relaxation, affords K-shell CEBEs that differ by an average of only 0.03 eV as compared to conventional def2-QZVP results (Table S2). For the def2-TZVP basis, the ΔSCF results change by an average of 0.4 eV upon uncontracting the basis set (Table S2), meaning that uncontracting the basis set is a good option when lower quality basis sets are used, in order to reach the basis-set limit more rapidly. For the purpose of this benchmark study, we use the conventional (contracted) def2-QZVP basis set because we subscribe to the idea that new theoretical methods should first be assessed near the basis-set limit before basis-set approximations are introduced, in order to avoid conflating method error with the basis-set error.[98] Calculations with generalized gradient approximation (GGA) functionals and their hybrids use the SG-1 quadrature grid,[99] whereas SG-2 is used for meta-GGA functionals.[100]

Calculations reported below were performed using a locally modified version of Q-Chem 5.4,[101] which contains several different

algorithms that can be used to optimize a non-*aufbau* determinant that contains a core hole or fractional core hole.[18] The simplest of these is the maximum overlap method (MOM),[82] and for the present calculations, we have found it sufficient to use the "initial MOM" (IMOM) algorithm.[83] This differs from the original MOM procedure only in that the reference orbitals used for computing overlaps are not updated during the SCF iterations, but are taken from an initial closed-shell, integer-occupancy SCF calculation that is used to obtain $E_0^{\text{initial}}(N)$ in Eq. (1). For the core-ionized states considered here, we find that IMOM avoids variational collapse in all cases.

Element-specific relativistic corrections from Ref. 102 were added to the absolute CEBEs: 0.14 eV for carbon, 0.28 eV for nitrogen, 0.51 eV for oxygen, and 0.85 eV for fluorine. (Similar values have been used in other recent studies of K-shell ionization.[39,103]) For molecules that have symmetry-equivalent atoms, the Boys localization procedure[104] is used prior to the ΔSCF and fractional-occupancy calculations.

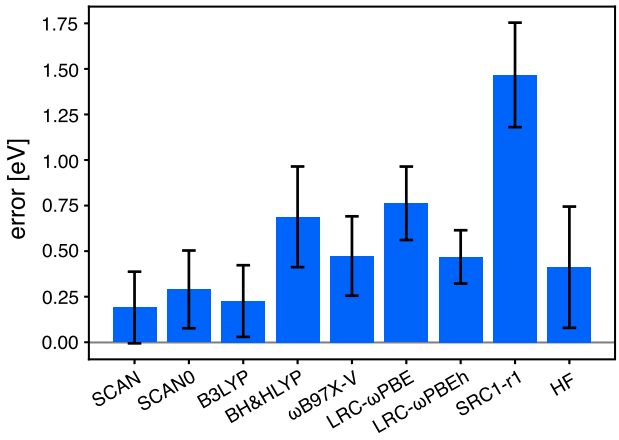

FIG. 1. MAEs for the CORE65 dataset obtained via ΔSCF calculations with different XC functionals. Whiskers represent ±1 standard deviation from the mean.

IV. RESULTS AND DISCUSSION

A. CORE65 dataset

Table II summarizes the accuracy of different functionals for CEBEs in the CORE65 test set as computed using ΔSCF, STM, and GSTM methods. (The ΔSCF errors are also summarized in Fig. 1.) For GSTM, we consider the $\mathcal{F}[0;3] + \mathcal{F}[1;3]$ $(n = 3)$ method in Table I. This requires four different SCF calculations and was considered also in Ref. 59. It has a leading error of $\mathcal{O}(E^{(5)}/54)$ that is lower, formally speaking, than any of the Slater-type methods that are listed in Table I and allows us to test the limits of the GSTM approach. Detailed results for the entire CORE65 dataset are supplied in the supplementary material (Tables S3–S5) and will be summarized here in terms of MAEs.

The best results are obtained from the SCAN functional whose MAE at the ΔSCF level is 0.2 eV with respect to the experiment, in accord with previous studies.[21] This is considerably better than the performance of the SRC1-r1 functional (MAE = 1.5 eV), which is notable since SRC1-r1 was specifically parameterized for K-edge excitation energies computed using time-dependent (TD-)DFT,[92] although not specifically for CEBEs. Ionization energies may present a more rigorous test, in which there is less opportunity for the cancellation of self-interaction between initial and final states since those two states have a different number of electrons in the case of a CEBE. It is interesting to note that the ΔSCF errors obtained using SCAN0 are slightly larger (MAE = 0.3 eV) as compared to the

TABLE II. MAEs (with respect to the experiment) for K-shell CEBEs in the CORE65 dataset using ΔSCF, STM, and GSTM methods. Within each row, the smallest error is shown in boldface and the largest error is italicized.

		Mean absolute error (eV)								
Element	Method	SCAN	SCAN0	B3LYP	BH & HLYP	ωB97X-V	LRC-ωPBE	LRC-ωPBEh	SRC1-r1	HFX
All	ΔSCF	**0.19**	0.29	0.23	0.69	0.47	0.76	0.47	*1.47*	0.41
C	ΔSCF	**0.13**	0.28	0.24	0.79	0.48	0.78	0.46	*1.65*	0.38
N	ΔSCF	**0.12**	0.22	0.14	0.61	0.45	0.79	0.46	*1.43*	0.35
O	ΔSCF	0.27	0.30	**0.23**	0.58	0.46	0.74	0.51	*1.25*	0.52
F	ΔSCF	0.54	0.56	0.36	0.80	0.57	0.60	0.34	*1.27*	**0.17**
All	STM	*2.71*	2.25	1.39	1.38	1.83	0.99	1.00	2.08	**0.45**
C	STM	*2.33*	2.03	1.32	1.43	1.74	0.84	0.90	2.22	**0.47**
N	STM	*2.67*	2.19	1.33	1.28	1.82	0.98	0.99	2.05	**0.33**
O	STM	*3.13*	2.49	1.49	1.33	1.93	1.17	1.10	1.92	**0.52**
F	STM	*3.71*	2.90	1.75	1.53	2.12	1.41	1.26	1.96	**0.24**
All	GSTM[a]	0.37	**0.15**	0.17	0.54	0.30	1.14	0.74	*1.36*	0.41
C	GSTM[a]	0.40	**0.12**	0.13	0.65	0.28	1.14	0.73	*1.58*	0.36
N	GSTM[a]	0.47	0.10	**0.16**	0.43	0.23	1.20	0.76	*1.19*	0.34
O	GSTM[a]	0.30	**0.21**	0.25	0.42	0.38	*1.12*	0.76	1.16	0.53
F	GSTM[a]	**0.15**	0.21	0.12	0.63	0.32	1.02	0.66	*1.09*	0.18

[a] $\mathcal{F}[0;3] + \mathcal{F}[1;3]$ $(n = 3)$ method from Table I.

semilocal SCAN functional and are closer to the B3LYP results. As compared to B3LYP or SCAN0, the BH & HLYP functional contains a larger fraction of HFX and also exhibits notably larger ΔSCF errors (MAE = 0.7 eV).

Other functionals, such as ωB97X-V, LRC-ωPBE, and LRC-ωPBEh, also afford larger ΔSCF errors as compared to SCAN, with MAEs of 0.5 eV for ωB97X-V and LRC-ωPBEh and 0.8 eV for LRC-ωPBE. Regarding the LRC functionals, it is interesting to note how the error is reduced by the addition of short-range HFX, yet neither functional is as accurate as HF theory itself. There is some precedent for this observation. In a recent ΔSCF study of K-, L-, and M-shell ionization energies of Ni and Cu atoms, it was found that HF calculations were more accurate than a broad array of density functionals,[29] although SCAN was not tested in that work. In Ref. 39, the hybrid functional PBEh(α) was applied to the CORE65 dataset, optimizing the fraction of HFX to minimize the errors. The optimal fraction was found to be $\alpha = 0.45$, affording an MAE of 0.33 eV that is only slightly better than HF theory (MAE = 0.41 eV).

We next address the performance of the STM and GSTM approaches, which are quite different (for a given functional) as compared to the ΔSCF results. The Slater-type methods are orbital-based estimates of CEBEs, rather than many-electron descriptions, and they depend on the accuracy of the Kohn–Sham one-particle energy levels. Both delocalization error (whose magnitude may be inferred by the performance of semilocal functionals) and localization error (as inferred by the performance of HF calculations) become critically important.

The performance of SCAN is considerably worse in the context of STM than it was for ΔSCF, and although GSTM improves the situation (as expected), its performance in conjunction with SCAN remains inferior to that of various hybrid and LRC functionals. In fact, the smallest STM errors are obtained using HF theory, suggesting issues with delocalization error, although the SCAN0 functional offers only a modest improvement upon SCAN results, and errors for STM-SCAN0 remain large (MAE = 2.25 eV). The situation is quite different for the GSTM approach, however. While the HF errors are virtually unchanged with respect to the corresponding STM results, both SCAN and the various hybrid functionals improve significantly. The accuracy of GSTM-SCAN is on par with that of HF theory whereas results with hybrid functionals are improved relative to HF theory, except in the case of the two LRC functionals. Although errors for the F(1s) subset defy some of these trends, we do not put much weight on that observation given that the CORE65 dataset contains only three data points for fluorine.

To further analyze the performance of the best of these methods, Fig. 2 plots absolute the CEBEs vs experiment using the ΔSCF, STM, and GSTM methods in conjunction with the SCAN functional. (The corresponding data computed using B3LYP are shown in Fig. S1.) The ΔSCF results follow the experimental trend line quite well, with little systematic error. In contrast, the STM and GSTM methods exhibit a roughly constant shift with respect to experiment, with STM calculations overestimating the CEBEs and GSTM results underestimating them by a smaller amount.

In view of these systematic trends, we tested an empirically shifted version of STM,

$$\mathrm{BE}_i \approx -\varepsilon_i(1/2) + \delta_i. \tag{25}$$

Here, $-\varepsilon_i(1/2)$ is the STM value of BE_i and δ_i is an empirical correction, computed according to

$$\delta_i = \beta[\varepsilon_i(1/2) - \varepsilon_i(0)], \tag{26}$$

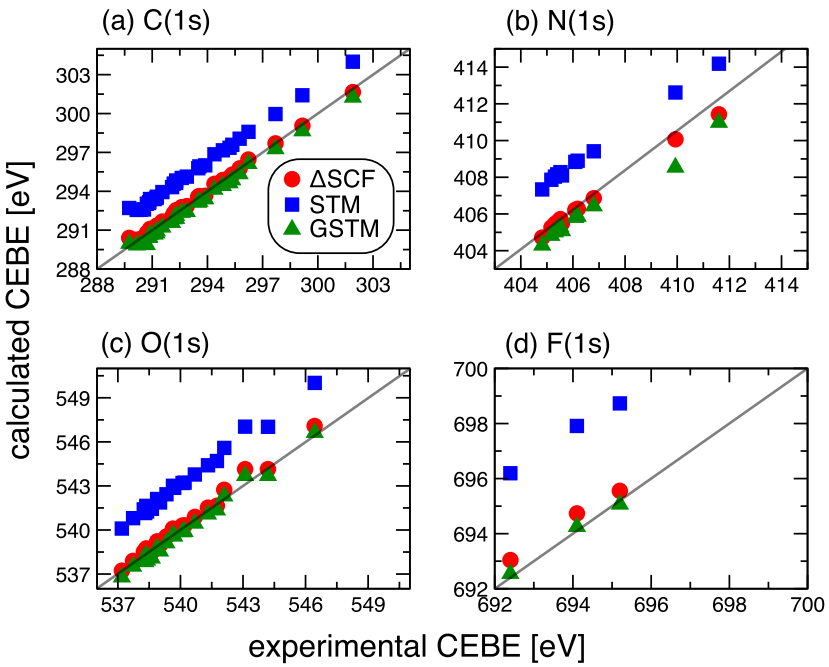

FIG. 2. Calculated CEBEs vs experiment, using the SCAN functional in conjunction with the ΔSCF, STM, and GSTM methods for (a) C(1s), (b) N(1s), (c) O(1s), and (d) F(1s) ionization energies in the CORE65 dataset.

where β is an empirical parameter whose value depends on the chosen XC functional. A correction of the form in Eq. (26) can be derived based on a Taylor expansion of $\varepsilon_i(q)$ around $q = 1/2$:

$$\left.\frac{\partial \varepsilon_i}{\partial q}\right|_{q=1/2} \approx \left.\frac{\Delta \varepsilon_i}{\Delta q}\right|_{q=1/2} = 2[\varepsilon_i(1/2) - \varepsilon_i(0)]. \tag{27}$$

This suggests a value of $\beta \approx 2$ although we treat β as a fitting parameter. Note that both $\varepsilon_i(0)$ and $\varepsilon_i(1/2)$ are already required for an STM calculation. The value $\varepsilon_i(0)$ comes from the integer-occupancy SCF calculation, and orbitals obtained from that calculation serve as a starting point for the fractional-occupancy SCF calculation that is used to obtain $\varepsilon_i(1/2)$. The correction δ_i can be understood to eliminate differential self-interaction in the localized electronic response between the initial state and the core-ionized state. At the same time, this correction compensates for higher order terms in the Taylor expansion of Eq. (7), which are omitted in the conventional STM.

Errors resulting from of this approach, for the CORE65 dataset and using best-fit values of β, are summarized in Table III. (See Table S6 for the full set of results.) The SCAN functional with $\beta = 3.2$ yields considerable improvement over unshifted STM-SCAN results, achieving a MAE of 0.15 eV that is smaller than the ΔSCF error (0.19 eV) for the same functional. The shift δ_i improves the results significantly for all functionals except HFX, although the best-fit value of β differs considerably from one functional to the next. Especially notable are BH & HLYP, where the MAE is reduced to 0.5 eV (better than the corresponding ΔSCF error) and SRC1-r1, for which the shifted STM error is 0.3 eV whereas the ΔSCF error is 1.5 eV. On the other hand, the SRC1-r1 functional requires a rather

TABLE III. Errors with respect to the experiment for K-shell CEBEs in the CORE65 dataset, computing using the empirically shifted STM approach.[a]

	Mean absolute error (eV)[b]								
Element	SCAN (β = 3.2)	SCAN0 (β = 4.7)	B3LYP (β = 2.1)	BH & HLYP (β = 8.8)	ωB97X-V (β = 3.2)	LRC-ωPBE (β = 1.2)	LRC-ωPBEh (β = 1.8)	SRC1-r1 (β = 15.2)	HFX (β = 0.2)
All	0.15	**0.14**	**0.14**	0.19	0.20	**0.14**	**0.14**	0.34	*0.44*
C	0.15	0.13	0.15	0.20	0.20	0.12	**0.11**	0.31	*0.55*
N	0.08	0.12	**0.04**	0.17	0.10	0.08	0.07	*0.37*	0.31
O	0.19	**0.18**	0.19	0.20	0.25	0.20	0.21	*0.39*	*0.39*
F	0.22	0.10	0.11	0.13	*0.30*	0.17	**0.09**	0.24	0.15

[a]Using Eq. (25) plus an element-specific relativistic correction.
[b]Largest and smallest errors are indicated in italics and bold, respectively.

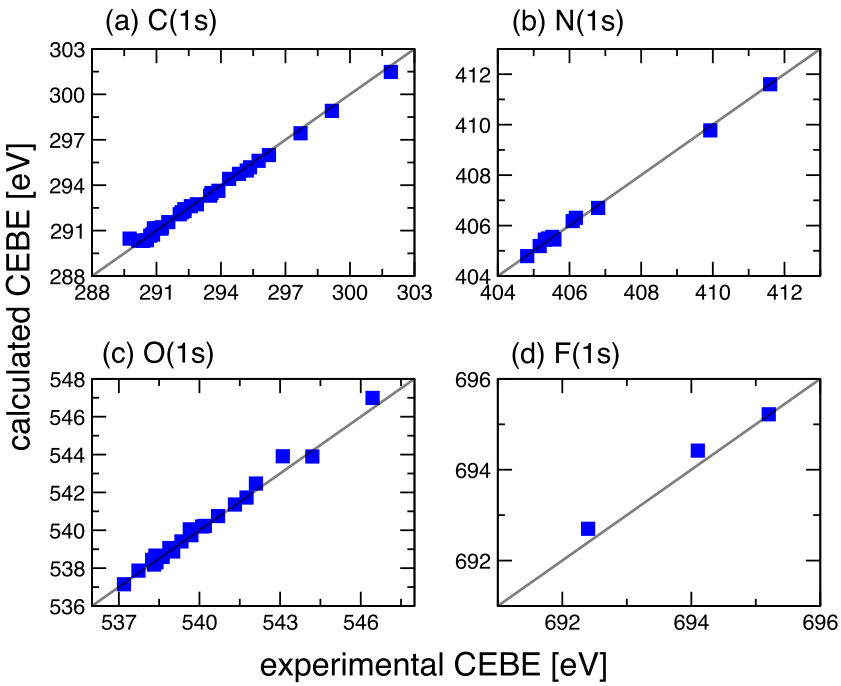

FIG. 3. K-shell CEBEs in the CORE65 dataset for (a) carbon, (b) nitrogen, (c) oxygen, and (d) fluorine, computed using an empirically shifted version of STM-SCAN, Eq. (25) with $\beta = 3.2$.

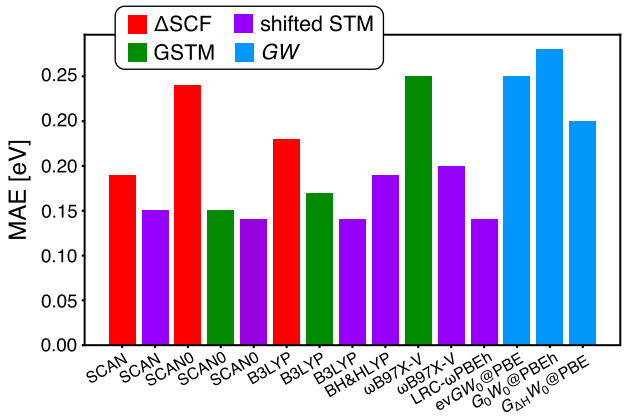

FIG. 4. MAEs for CORE65 test set according to some of the best-performing methods. In some cases, results from more than one (color-coded) method are shown for the same XC functional. Error statistics for the *GW* methods are taken from Refs. 39 and 40.

large fitting parameter ($\beta = 15.2$) in order to achieve this result. Safer bets are the shifted STM-SCAN and shifted STM-B3LYP methods, for which absolute CEBEs are plotted vs experiment in Fig. 3 and Fig. S2, respectively.

A survey of the errors obtained using several of the best methods (including ΔSCF, GSTM, and empirically shifted STM with various functionals) is presented in Fig. 4, alongside results from several variants of the *GW* method, which have recently been tested using the same dataset.[39,40] The shifted-STM approach achieves a MAE of 0.14 eV in conjunction with any of several different functionals: SCAN0, B3LYP, LRC-ωPBE, and LRC-ωPBEh. This is actually slightly smaller than the MAE obtained using a variety of (considerably more expensive) *GW* methods. The latter include the non-self-consistent variant G_0W_0@PBEh(α), whose MAE is 0.33 eV, the "eigenvalue self-consistent" evGW_0@PBE approach (MAE = 0.30 eV), and *GW* with Hedin shift, $G_{\Delta H}W_0$@PBE,[40] whose MAE is 0.25 eV. Moreover, these *GW* methods are not free from empiricism. For example, G_0W_0@PBEh(α) uses a fraction of HFX ($\alpha = 0.45$) that has been adjusted in order to minimize errors with respect to experimental CEBEs.[39] GSTM methods based on the SCAN0, B3LYP, and ωB97X-V also yield similar accuracy as compared to the *GW* methods.

B. K-shell CEBEs for other molecules

To test the shifted-STM approach beyond the CORE65 dataset, we next consider C(1s) ionization of ethyl trifluoroacetate. This molecule has four carbon atoms whose K-shell ionization energies are distinguishable, and as such it has been historically important in understanding XPS chemical shifts.[105] This molecule has also been used to benchmark various theoretical methods.[17,40,106,108,109] Our own results for ethyl trifluoroacetate are listed in Table IV alongside *GW* results from the literature.[40,106] The SRC1-r1 and HFX functionals are not considered due to their relatively large errors in shifted-STM calculations.

Among the *GW* methods, the evGW_0@PBE approach affords the smallest MAE with respect to the experiment, 0.2 eV. The ΔSCF calculations using SCAN, SCAN0, and B3LYP are also quite accurate, but errors are larger for eliminate spaces in the acronym BH&HLYP (MAE = 0.8 eV). Note that the absolute CEBEs in our SCAN results are slightly different from those reported in Ref. 17 where a numerical orbital representation was used, but the differences do not concern us given the SCAN functional's well-known sensitivity to the quality of the numerical integration grid.[110–112]

As applied to ethyl trifluoroacetate, the original STM approach exhibits errors of 1–2 eV for some of the functionals tested. However, shifted-STM values (using β parameters optimized for the CORE65 test set) exhibit errors that are smaller than those obtained using *GW* methods. The best shifted-STM results are obtained with the LRC-ωPBEh functional, with a maximum error of only 0.04 eV for the four C(1s) ionization energies. However, none of the functionals considered in Table IV exhibit any errors larger than 0.17 eV. The β parameters therefore appear to be transferrable, which is not altogether surprising given the element-specific nature of XPS.

Finally, we tested the performance of the shifted-STM approach for the adenine and thymine molecules, for which benchmark theoretical values are available at the level of fourth-order algebraic-diagrammatic construction [ADC(4)].[113] Error statistics comparing the shifted-STM approach to these benchmarks are summarized in Table V, where the dataset includes seven N(1s) CEBEs, ten C(1s) CEBEs, and two O(1s) CEBEs, corresponding to all of the heavy atoms in adenine and thymine. (The full set of calculated CEBEs can be found in the supplementary material.) Our results suggest that shifted-STM methods from various density functionals improve considerably upon the conventional STM approach with minimal empiricism. As a result of the empirical correction, this method is even able to improve upon ΔSCF results.

C. VtC x-ray emission

As a rather different application, we consider the usefulness of the STM approach for VtC transitions in x-ray emission spectroscopy (VtC-XES), which is beginning to attract attention within the quantum chemistry community.[114–121] This application represents a first step in extending Slater-type approaches to core-excited rather than core-ionized states. Within the context of DFT, VtC-XES is typically simulated by applying linear-response TD-DFT to a reference determinant that contains a core hole,[114,120] as a ΔSCF approach would require state-by-state constrained SCF calculations to place an electron in each of the valence virtual orbitals. In contrast, using STM with just two SCF calculations, one can obtain the entire spectrum. The first calculation computes conventional integer-occupancy SCF orbitals, which are used as a starting point for a fractional-occupancy calculation with $n_i = 1/2$ in the core 1s orbital. A full spectrum of excitation energies is computed from that calculation using the formula

$$\Delta E_{i\to a} = \varepsilon_a(1/2) - \varepsilon_i(1/2), \tag{28}$$

in which both eigenvalues are computed from the same fractional-electron calculation. The integer-occupancy calculation can be

TABLE IV. Errors in the four C(1s) ionization energies of the ethyl trifluoroacetate molecule.

Method	Functional	Individual errors (eV)[a]				Overall (eV)	
		C1	C2	C3	C4	Mean	Max
evGW_0[b]	PBE	−0.70	−0.54	−0.19	−0.12	−0.36	0.36
evGW_0[c]	PBE	−0.41	−0.18	−0.04	−0.09	−0.18	0.18
G_0W_0[b]	PBEh(α = 0.45)	0.56	0.54	0.30	0.16	0.39	0.39
$G_{\Delta H}W_0$[b]	PBE	−0.53	−0.44	−0.10	−0.02	−0.27	0.27
ΔSCF	SCAN	−0.24	−0.17	−0.03	0.08	−0.09	0.13
STM	SCAN	2.13	2.17	2.30	2.35	2.24	2.24
GSTM	SCAN	−2.41	−2.30	−2.38	−2.33	−2.35	2.35
STM (shifted)[d]	SCAN	−0.28	−0.20	−0.05	−0.01	−0.14	0.14
ΔSCF	SCAN0	0.23	0.32	0.18	0.21	0.23	0.23
STM	SCAN0	2.08	2.15	1.97	1.94	2.03	2.03
GSTM	SCAN0	−0.03	0.06	−0.11	−0.10	−0.05	0.07
STM (shifted)[d]	SCAN0	0.01	0.12	0.00	−0.06	−0.02	0.05
ΔSCF	B3LYP	−0.01	0.11	0.11	0.20	0.10	0.11
STM	B3LYP	1.15	1.26	1.22	1.26	1.22	1.22
GSTM	B3LYP	−0.29	−0.15	−0.16	−0.07	−0.17	0.17
STM (shifted)[d]	B3LYP	−0.04	0.08	0.06	0.09	0.05	0.07
ΔSCF	BH & HLYP	0.90	1.05	0.63	0.61	0.80	0.80
STM	BH & HLYP	1.62	1.75	1.28	1.21	1.47	1.47
GSTM	BH & HLYP	0.75	0.91	0.50	0.47	0.66	0.66
STM (shifted)[d]	BH & HLYP	0.19	0.36	0.02	−0.10	0.12	0.17
ΔSCF	ωB97X-V	0.33	0.49	0.39	0.42	0.41	0.41
STM	ωB97X-V	1.68	1.82	1.68	1.67	1.71	1.71
GSTM	ωB97X-V	0.11	0.28	0.17	0.21	0.19	0.19
STM (shifted)[d]	ωB97X-V	0.10	0.26	0.17	0.14	0.17	0.17
ΔSCF	LRC-ωPBE	−1.10	−0.94	−0.85	−0.78	−0.92	0.92
STM	LRC-ωPBE	0.61	0.75	0.80	0.81	0.74	0.74
GSTM	LRC-ωPBE	−1.48	−1.30	−1.22	−1.14	−1.29	1.29
STM (shifted)[d]	LRC-ωPBE	−0.20	−0.05	0.00	0.01	−0.06	0.07
ΔSCF	LRC-ωPBEh	−0.6	−0.54	−0.54	−0.48	−0.56	0.56
STM	LRC-ωPBEh	0.76	0.88	0.84	0.84	0.83	0.83
GSTM	LRC-ωPBEh	−0.99	−0.83	−0.83	−0.77	−0.85	0.85
STM (shifted)[d]	LRC-ωPBEh	−0.12	0.02	0.00	−0.01	−0.03	0.04
Experiment[e]		299.45	296.01	293.07	291.20		
Experiment[f]		298.93	295.80	293.19	291.47		

[a]With respect to experimental values from Ref. 105.
[b]From Ref. 40.
[c]From Ref. 106.
[d]Using β from Table III.
[e]From Ref. 107.
[f]From Ref. 105.

reused for different spectra but a different fractional-electron calculation is needed for each occupied orbital i that is excited. All final states (virtual orbitals a) are obtained from the same calculation.

Results are shown for several small molecules in Table VI for VtC transitions of second-row elements where reliable experimental data are available. No empirical shift has been employed; nevertheless, results obtained using the B3LYP functional are quite good, with an MAE of 0.8 eV. This can be compared to results for the same dataset that have been obtained using many-body methods including EOM-CCSD (MAE = 0.5 eV) and ADC (MAEs ranging from 0.3 to 1.5 eV depending on the particular variant of ADC).[119] It is possible that the STM results might be improved further by empirical shifting, and we hope to provide a more complete evaluation of (G)STM methods for core-excited states in due course.

TABLE V. Error statistics in K-shell CEBEs for adenine and thymine, as compared to ADC(4) benchmarks.[a]

Functional	Method	MAE (eV)[b] Adenine	Thymine
SCAN	ΔSCF	0.17	0.24
SCAN	STM	2.28	2.49
SCAN	GSTM	0.63	0.46
SCAN	Shifted-STM[c]	0.19	**0.20**
SCAN0	ΔSCF	0.19	0.41
SCAN0	STM	1.91	2.12
SCAN0	GSTM	0.28	0.19
SCAN0	Shifted-STM[c]	0.14	0.23
B3LYP	ΔSCF	0.15	0.22
B3LYP	STM	1.05	1.23
B3LYP	GSTM	1.52	0.27
B3LYP	Shifted-STM[c]	0.13	0.23
BH & HLYP	ΔSCF	0.41	0.64
BH & HLYP	STM	1.04	1.18
BH & HLYP	GSTM	0.27	0.56
BH & HLYP	Shifted-STM[c]	0.17	0.37
ωB97X-V	ΔSCF	0.41	0.61
ωB97X-V	STM	1.58	1.77
ωB97X-V	GSTM	0.14	0.31
ωB97X-V	Shifted-STM[c]	0.13	0.36
LRC-ωPBE	ΔSCF	1.00	0.84
LRC-ωPBE	STM	0.73	0.90
LRC-ωPBE	GSTM	1.36	1.22
LRC-ωPBE	Shifted-STM[c]	0.13	**0.20**
LRC-ωPBEh	ΔSCF	0.68	0.52
LRC-ωPBEh	STM	0.75	0.91
LRC-ωPBEh	GSTM	0.96	0.82
LRC-ωPBEh	Shifted-STM[c]	**0.12**	0.23

[a]Benchmarks from Ref. 113.
[b]Smallest MAEs are shown in boldface.
[c]Using β from Table III.

V. CONCLUSIONS

We have quantified the performance of various density-functional approaches for computing K-shell electron binding energies corresponding to the ionization of C(1s), O(1s), N(1s), and F(1s) orbitals. As a baseline (for any given functional), we provide comprehensive benchmarks for the ΔSCF or "full core hole" approach, although our real interest lies in methods based on Slater's transition concept using fractional-occupancy SCF calculations. This provides a means to compute core-level transition energies directly from Kohn–Sham orbital energy levels and may offer more chemical insight into the nature of chemical shifts in x-ray transitions, which could be rationalized in terms of shifting MO energy levels. The convenience of STM-based methods also represents a first step toward modeling transient x-ray experiments directly in terms of one-particle energy levels.

TABLE VI. VtC-XES results (in eV) using STM(B3LYP), as compared to experiment.

Molecule	Transition	Expt.[a]	STM error
CH_4	$1t_2 \rightarrow 1a_1$	276.3	−0.2
CH_3OH	$2a'' \rightarrow 2a'$	281.2	0.8
	$7a' \rightarrow 2a'$	279.5	0.6
	$6a' \rightarrow 2a'$	277.4	−0.3
NH_3	$2a_1 \rightarrow 1a_1$	395.1	−1.7
	$1e \rightarrow 1a_1$	388.8	−0.3
H_2O	$1b_1 \rightarrow 1a_1$	527.1	−1.8
	$3a_1 \rightarrow 1a_1$	525.4	−1.9
	$1b_2 \rightarrow 1a_1$	521.0	−1.2
CH_3OH	$2a'' \rightarrow 1a'$	527.8	−0.7
	$7a' \rightarrow 1a'$	526.1	0.2
	$6a' \rightarrow 1a'$	523.9	−0.2
C_2H_5OH	$3a'' \rightarrow 1a'$	528.0	−0.4
	$10a' \rightarrow 1a'$	526.4	−0.1
CH_3F	$2e \rightarrow 1a_1$	678.6	0.6
	$5a_1 \rightarrow 1a_1$	675.6	−0.9

[a]Taken from Ref. 119.

When used with the SCAN or B3LYP functionals, the baseline ΔSCF procedure achieves an MAE of 0.2 eV as compared to experiment (upon inclusion of atomic relativistic corrections and using a converged basis set), which is more accurate than other functionals tested, although SCAN0 is competitive and ωB97X-V exhibits a MAE of 0.5 eV. The SRC1-r1 functional performs surprisingly poorly (MAE = 1.5 eV), despite having been parameterized for K-edge XAS using TD-DFT. STM-based methods are significantly less accurate but GSTM methods, which use more than one fractional-electron SCF calculation, can achieve MAEs of 0.2–0.3 eV for the same dataset, using functionals including SCAN0, B3LYP, or ωB97X-V.

Most importantly, we find that an empirically shifted version of the conventional STM reduces the aforementioned errors below 0.2 eV for a variety of functionals. This approach requires only two SCF calculations: a conventional one for the ground state of the neutral molecule, followed by a single, edge-specific fractional-electron calculation for the core-ionized state. This is a cost comparable to that of ΔSCF and affords accuracy that is competitive with the best variants of *GW*, all of which are considerably more expensive. Tests for a variety of main-group compounds suggest that this shifted-STM approach affords accurate chemical shifts as well.

Together, these results suggest that the shifted-STM technique is a useful computational tool, especially in cases where *GW* or ΔSCF calculations are expensive or otherwise inconvenient. It is also of interest to extend this method to core-excited states rather than the core-ionized states that are primarily considered here. As a first step in that direction, we report VtC-XES transitions for a benchmark set of molecules. Even without empirical shifting, STM results are

competitive with many-body theory. Unlike ΔSCF, this approach allows for a spectrum of transitions to be computed in a single shot, similar to TD-DFT but without the need for large shifts in the excitation energies[122] or specialized functionals.[92] We will report more fully on this approach in the future.

SUPPLEMENTARY MATERIAL

See the supplementary material for the complete dataset for all methods tested.

ACKNOWLEDGMENTS

This work was supported by the U.S. Department of Energy, Office of Basic Energy Sciences, Division of Chemical Sciences, Geosciences, and Biosciences (Award No. DE-SC0008550), and by the National Science Foundation (Grant No. CHE-1955282). Calculations were performed at the Ohio Supercomputer Center.[123] S.J. thanks Dr. Kevin Carter-Fenk for help with Q-Chem.

AUTHOR DECLARATIONS

Conflict of Interest

J.M.H. serves on the board of directors of Q-Chem Inc.

Author Contributions

Subrata Jana: Formal analysis (equal); Investigation (lead); Methodology (equal); Software (lead); Writing – original draft (lead); Writing – review & editing (supporting). **John M. Herbert**: Conceptualization (lead); Data curation (equal); Funding acquisition (lead); Project administration (lead); Resources (lead); Supervision (lead); Writing – review & editing (lead).

DATA AVAILABILITY

The data that support the findings of this study are available within the article and its supplementary material.

REFERENCES

[1] F. de Groot and A. Kotani, *Core Level Spectroscopy of Solids* (CRC Press, Boca Raton, 2008).
[2] C. S. Fadley, "X-ray photoelectron spectroscopy: Progress and perspectives," J. Electron Spectrosc. **178–179**, 2–32 (2010).
[3] P. S. Bagus, E. S. Ilton, and C. J. Nelin, "The interpretation of XPS spectra: Insights into materials properties," Surf. Sci. Rep. **68**, 273–304 (2013).
[4] A. Aarva, V. L. Deringer, S. Sainio, T. Laurila, and M. A. Caro, "Understanding x-ray spectroscopy of carbonaceous materials by combining experiments, density functional theory, and machine learning. Part I: Fingerprint spectra," Chem. Mater. **31**, 9243–9255 (2019).
[5] A. Aarva, V. L. Deringer, S. Sainio, T. Laurila, and M. A. Caro, "Understanding x-ray spectroscopy of carbonaceous materials by combining experiments, density functional theory, and machine learning. Part II: Quantitative fitting of spectra," Chem. Mater. **31**, 9256–9267 (2019).
[6] P. S. Bagus, F. Illas, G. Pacchioni, and F. Parmigiani, "Mechanisms responsible for chemical shifts of core-level binding energies and their relationship to chemical bonding," J. Electron Spectrosc. **100**, 215–236 (1999).
[7] R. Haerle, E. Riedo, A. Pasquarello, and A. Balderschi, "sp^2/sp^3 hybridization ratio in amorphous carbon from C 1*s* core-level shifts: X-ray photoelectron spectroscopy and first-principles calculation," Phys. Rev. B **65**, 045101 (2001).
[8] P. D. C. King, T. D. Veal, C. F. McConville, F. Fuchs, J. Furthmüller, F. Bechstedt, J. Schörmann, D. J. As, K. Lischka, H. Lu, and W. J. Schaff, "Valence band density of states of zinc-blende and wurtzite InN from x-ray photoemission spectroscopy and first-principles calculations," Phys. Rev. B **77**, 115213 (2008).
[9] C. Körber, V. Krishnakumar, A. Klein, G. Panaccione, P. Torelli, A. Walsh, J. L. F. Da Silva, S.-H. Wei, R. G. Egdell, and D. J. Payne, "Electronic structure of In_2O_3 and Sn-doped In_2O_3 by hard x-ray photoemission spectroscopy," Phys. Rev. B **81**, 165207 (2010).
[10] J. Bandlow, P. Kaghazchi, T. Jacob, C. Papp, B. Tränkenschuh, R. Streber, M. P. A. Lorenz, T. Fuhrmann, R. Denecke, and H.-P. Steinrück, "Oxidation of stepped Pt(111) studied by x-ray photoelectron spectroscopy and density functional theory," Phys. Rev. B **83**, 174107 (2011).
[11] J. M. Kahk, C. G. Poll, F. E. Oropeza, J. M. Ablett, D. Céolin, J.-P. Rueff, S. Agrestini, Y. Utsumi, K. D. Tsuei, Y. F. Liao, F. Borgatti, G. Panaccione, A. Regoutz, R. G. Egdell, B. J. Morgan, D. O. Scanlon, and D. J. Payne, "Understanding the electronic structure of IrO_2 using hard-x-ray photoelectron spectroscopy and density-functional theory," Phys. Rev. Lett. **112**, 117601 (2014).
[12] F. Viñes, C. Sousa, and F. Illas, "On the prediction of core level binding energies in molecules, surfaces and solids," Phys. Chem. Chem. Phys. **20**, 8403–8410 (2018).
[13] A. Regoutz, A. M. Ganose, L. Blumenthal, C. Schlueter, T.-L. Lee, G. Kieslich, A. K. Cheetham, G. Kerherve, Y.-S. Huang, R.-S. Chen, G. Vinai, T. Pincelli, G. Panaccione, K. H. L. Zhang, R. G. Egdell, J. Lischner, D. O. Scanlon, and D. J. Payne, "Insights into the electronic structure of OsO_2 using soft and hard x-ray photoelectron spectroscopy in combination with density functional theory," Phys. Rev. Mater. **3**, 025001 (2019).
[14] A. Regoutz, M. S. Wolinska, N. K. Fernando, and L. E. Ratcliff, "A combined density functional theory and x-ray photoelectron spectroscopy study of the aromatic amino acids," Electron. Struct. **2**, 044005 (2021).
[15] N. A. Besley, "Density functional theory based methods for the calculation of x-ray spectroscopy," Acc. Chem. Res. **53**, 1306–1315 (2020).
[16] N. A. Besley, "Modeling of the spectroscopy of core electrons with density functional theory," Wiley Interdiscip. Rev.: Comput. Mol. Sci. **12**, e1527 (2021).
[17] B. P. Klein, S. J. Hall, and R. J. Maurer, "The nuts and bolts of core-hole constrained *ab initio* simulation for *K*-shell x-ray photoemission and absorption spectra," J. Phys.: Condens. Matter **33**, 154005 (2021).
[18] J. M. Herbert, "Density functional theory for electronic excited states," in *Theoretical and Computational Photochemistry: Fundamentals, Methods, Applications and Synergy with Experimental Approaches*, edited by C. García-Iriepa and M. Marazzi (Elsevier, 2023), Chap. 3 (in press; preprint available at DOI: 10.48550/arXiv.2204.10135).
[19] N. A. Besley, A. T. B. Gilbert, and P. M. W. Gill, "Self-consistent-field calculations of core excited states," J. Chem. Phys. **130**, 124308 (2009).
[20] N. P. Bellafont, G. A. Saiz, F. Viñes, and F. Illas, "Performance of Minnesota functionals on predicting core-level binding energies of molecules containing main-group elements," Theor. Chem. Acc. **135**, 35 (2016).
[21] J. M. Kahk and J. Lischner, "Accurate absolute core-electron binding energies of molecules, solids, and surfaces from first-principles calculations," Phys. Rev. Mater. **3**, 100801(R) (2019).
[22] J. M. Kahk, G. S. Michelitsch, R. J. Maurer, K. Reuter, and J. Lischner, "Core electron binding energies in solids from periodic all-electron Δ-self-consistent-field calculations," J. Phys. Chem. Lett. **12**, 9353–9359 (2021).
[23] M. A. Ambroise, A. Dreuw, and F. Jensen, "Probing basis set requirements for calculating core ionization and core excitation spectra using correlated wave function methods," J. Chem. Theory Comput. **17**, 2832–2842 (2021).
[24] J. M. Kahk and J. Lischner, "Predicting core electron binding energies in elements of the first transition series using the Δ-self-consistent-field method," Faraday Discuss. **236**, 364–373 (2022).
[25] D. Hait and M. Head-Gordon, "Excited state orbital optimization via minimizing the square of the gradient: General approach and application to singly and doubly excited states via density functional theory," J. Chem. Theory Comput. **16**, 1699–1710 (2020).
[26] K. Carter-Fenk and J. M. Herbert, "State-targeted energy projection: A simple and robust approach to orbital relaxation of non-aufbau self-consistent field solutions," J. Chem. Theory Comput. **16**, 5067–5082 (2020).

[27]L. Triguero, O. Plashkevych, L. G. M. Pettersson, and H. Ågren, "Separate state vs transition state Kohn–Sham calculations of x-ray photoelectron binding energies and chemical shifts," J. Electron Spectrosc. **104**, 195–207 (1999).
[28]N. P. Bellafont, P. S. Bagus, and F. Illas, "Prediction of core level binding energies in density functional theory: Rigorous definition of initial and final state contributions and implications on the physical meaning of Kohn–Sham energies," J. Chem. Phys. **142**, 214102 (2015).
[29]J. V. Jorstad, T. Xie, and C. M. Morales, "Δ-SCF calculations of core electron binding energies in first-row transition metal atoms," Int. J. Quantum Chem. **122**, e26881 (2022).
[30]J. Sun, A. Ruzsinszky, and J. P. Perdew, "Strongly constrained and appropriately normed semilocal density functional," Phys. Rev. Lett. **115**, 036402 (2015).
[31]L. A. Cunha, D. Hait, R. Kang, Y. Mao, and M. Head-Gordon, "Relativistic orbital-optimized density functional theory for accurate core-level spectroscopy," J. Phys. Chem. Lett. **13**, 3438–3449 (2022).
[32]J. Liu, D. Matthews, S. Coriani, and L. Cheng, "Benchmark calculations of K-edge ionization energies for first-row elements using scalar-relativistic core–valence-separated equation-of-motion coupled-cluster methods," J. Chem. Theory Comput. **15**, 1642–1651 (2019).
[33]X. Zheng and L. Cheng, "Performance of delta-coupled-cluster methods for calculations of core-ionization energies of first-row elements," J. Chem. Theory Comput. **15**, 4945–4955 (2019).
[34]M. Nooijen and R. J. Bartlett, "Description of core-excitation spectra by the open-shell electron-attachment equation-of-motion coupled cluster method," J. Chem. Phys. **102**, 6735–6756 (1995).
[35]M. P. Coons and J. M. Herbert, "Quantum chemistry in arbitrary dielectric environments: Theory and implementation of nonequilibrium Poisson boundary conditions and application to compute vertical ionization energies at the air/water interface," J. Chem. Phys. **148**, 222834 (2018).
[36]A. Dreuw and T. Fransson, "Using core-hole reference states for calculating x-ray photoelectron and emission spectra," Phys. Chem. Chem. Phys. **24**, 11259–11267 (2022).
[37]L. Reining, "The GW approximation: Content, successes and limitations," Wiley Interdiscip. Rev.: Comput. Mol. Sci. **8**, e1344 (2018).
[38]D. Golze, J. Wilhelm, M. J. van Setten, and P. Rinke, "Core-level binding energies from *GW*: An efficient full-frequency approach within a localized basis," J. Chem. Theory Comput. **14**, 4856–4869 (2018).
[39]D. Golze, L. Keller, and P. Rinke, "Accurate absolute and relative core-level binding energies from *GW*," J. Phys. Chem. Lett. **11**, 1840–1847 (2020).
[40]J. Li, Y. Jin, P. Rinke, W. Yang, and D. Golze, "Benchmark of *GW* methods for core-level binding energies," J. Chem. Theory Comput. **18**, 7570–7585 (2022).
[41]S. J. Bintrim and T. C. Berkelbach, "Full-frequency GW without frequency," J. Chem. Phys. **154**, 041101 (2021).
[42]R. Quintero-Monsebaiz, E. Monino, A. Marie, and P.-F. Loos, "Connections between many-body perturbation and coupled-cluster theories," J. Chem. Phys. **157**, 231102 (2022).
[43]M. J. van Setten, F. Caruso, S. Sharifzadeh, X. Ren, M. Scheffler, F. Liu, J. Lischner, L. Lin, J. R. Deslippe, S. G. Louie, C. Yang, F. Weigend, J. B. Neaton, F. Evers, and P. Rinke, "*GW*100: Benchmarking G_0W_0 for molecular systems," J. Chem. Theory Comput. **11**, 5665–5687 (2015).
[44]M. Govoni and G. Galli, "GW100: Comparison of methods and accuracy of results obtained with the WEST code," J. Chem. Theory Comput. **14**, 1895–1909 (2018).
[45]P. Koval, D. Foerster, and D. Sánchez-Portal, "Fully self-consistent *GW* and quasiparticle self-consistent *GW* for molecules," Phys. Rev. B **89**, 155417 (2014).
[46]P.-F. Loos, P. Romaniello, and J. A. Berger, "Green functions and self-consistency: Insights from the spherium model," J. Chem. Theory Comput. **14**, 3071–3082 (2018).
[47]T. Körzdörfer and N. Marom, "Strategy for finding a reliable starting point for G_0W_0 demonstrated for molecules," Phys. Rev. B **86**, 041110R (2012).
[48]F. Bruneval and M. A. L. Marques, "Benchmarking the starting points of the *GW* approximation for molecules," J. Chem. Theory Comput. **9**, 324–329 (2013).
[49]T. Tsudeda, J.-W. Song, S. Suzuki, and K. Hirao, "On Koopmans' theorem in density functional theory," J. Chem. Phys. **133**, 174101 (2010).
[50]K. Hirao, T. Nakajima, B. Chan, J.-W. Song, and H.-S. Bae, "Core-level excitation energies of nucleic acid bases expressed as orbital energies of the Kohn–Sham density functional theory with long-range corrected functionals," J. Phys. Chem. A **124**, 10482–10494 (2020).
[51]K. Hirao, H.-S. Bae, J.-W. Song, and B. Chan, "Koopmans'-type theorem in Kohn–Sham theory with optimally tuned long-range-corrected (LC) functionals," J. Phys. Chem. A **125**, 3489–3502 (2021).
[52]G. Tu, V. Carravetta, O. Vahtras, and H. Ågren, "Core ionization potentials from self-interaction corrected Kohn–Sham orbital energies," J. Chem. Phys. **127**, 174110 (2007).
[53]Y. Imamura and H. Nakai, "Description of core-ionized and core-excited states by density functional theory and time-dependent density functional theory," in *Quantum Systems in Chemistry and Physics: Progress in Theoretical Chemistry and Physics*, edited by K. Nishikawa, J. Maruani, E. J. Brändas, G. Delgado-Barrio, and P. Piecuch (Spring Science + Business Media, Dordrecht, 2012), Vol. 26, Chap. 14, pp. 275–308.
[54]S. Akter, Y. Yamamoto, C. M. Diaz, K. A. Jackson, R. R. Zope, and T. Baruah, "Study of self-interaction errors in density functional predictions of dipole polarizabilities and ionization energies of water clusters using Perdew–Zunger and locally scaled self-interaction corrected methods," J. Chem. Phys. **153**, 164304 (2020).
[55]S. Adhikari, B. Santra, S. Ruan, P. Bhattarai, N. K. Nepal, K. A. Jackson, and A. Ruzsinszky, "The Fermi–Löwdin self-interaction correction for ionization energies of organic molecules," J. Chem. Phys. **153**, 184303 (2020).
[56]J. C. Slater and J. H. Wood, "Statistical exchange and the total energy of a crystal," Int. J. Quantum Chem. **5**, 3–34 (1971).
[57]J. C. Slater, "Statistical exchange-correlation in the self-consistent field," Adv. Quantum Chem. **6**, 1–92 (1972).
[58]A. R. Williams, R. A. deGroot, and C. B. Sommers, "Generalization of Slater's transition state concept," J. Chem. Phys. **63**, 628–631 (1975).
[59]K. Hirao, T. Nakajima, and B. Chan, "An improved Slater's transition state approximation," J. Chem. Phys. **155**, 034101 (2021).
[60]T. Nakajima, K. Hirao, and B. Chan, "Higher-order transition state approximation," J. Chem. Phys. **156**, 114112 (2022).
[61]K. Schwarz, "On Slater's transition state for ionization energies," Chem. Phys. **7**, 100–107 (1975).
[62]D. P. Chong, "Accurate calculation of core-electron binding energies by the density-functional method," Chem. Phys. Lett. **232**, 486–490 (1995).
[63]G. Cavigliasso and D. P. Chong, "Accurate density-functional calculation of core-electron binding energies by a total-energy difference approach," J. Chem. Phys. **111**, 9485–9492 (1999).
[64]Y. Zhang and W. Yang, "Perspective on 'Density-functional theory for fractional particle number: Derivative discontinuities of the energy,'" Theor. Chem. Acc. **103**, 346–348 (2000).
[65]W. Yang, Y. Zhang, and P. W. Ayers, "Degenerate ground states and a fractional number of electrons in density and reduced density matrix functional theory," Phys. Rev. Lett. **84**, 5172–5174 (2000).
[66]A. J. Cohen, P. Mori-Sánchez, and W. Yang, "Fractional spins and static correlation error in density functional theory," J. Chem. Phys. **129**, 121104 (2008).
[67]J. P. Perdew, R. G. Parr, M. Levy, and J. L. Balduz, Jr., "Density-functional theory for fractional particle number: Derivative discontinuities of the energy," Phys. Rev. Lett. **49**, 1691–1694 (1982).
[68]J. P. Perdew and M. Levy, "Physical content of the exact Kohn–Sham orbital energies: Band gaps and derivative discontinuities," Phys. Rev. Lett. **51**, 1884–1887 (1983).
[69]A. J. Cohen, P. Mori-Sanchez, and W. Yang, "Insights into current limitations of density functional theory," Science **321**, 792–794 (2008).
[70]A. Görling, "Exchange-correlation potentials with proper discontinuities for physically meaningful Kohn–Sham eigenvalues and band structures," Phys. Rev. B **91**, 245120 (2015).
[71]B. Sadigh, P. Erhart, and D. Åberg, "Variational polaron self-interaction-corrected total-energy functional for charge excitations in insulators," Phys. Rev. B **92**, 075202 (2015).
[72]A. Bajaj, J. P. Janet, and H. J. Kulik, "Communication: Recovering the flat-plane condition in electronic structure theory at semi-local DFT cost," J. Chem. Phys. **147**, 191101 (2017).

[73]S. N. Steinmann and W. Yang, "Wave function methods for fractional electrons," J. Chem. Phys. **139**, 074107 (2013).
[74]M. Simons and D. A. Matthews, "Transition-potential coupled cluster," J. Chem. Phys. **154**, 014106 (2021).
[75]M. Simons and D. A. Matthews, "Transition-potential coupled cluster II: Optimisation of the core orbital occupation number," Mol. Phys. e2088421 (published online).
[76]R. Geneaux, H. J. B. Marroux, A. Guggenmos, D. M. Neumark, and S. R. Leone, "Transient absorption spectroscopy using high harmonic generation: A review of ultrafast x-ray dynamics in molecules and solids," Philos. Trans. R. Soc., A **377**, 20170463 (2019).
[77]H. Liu, I. M. Klein, J. M. Michelsen, and S. K. Cushing, "Element-specific electronic and structural dynamics using transient XUV and soft x-ray spectroscopy," Chem **7**, 2569–2584 (2021).
[78]S. M. Cavaletto, D. R. Nascimento, Y. Zhang, N. Govind, and S. Mukamel, "Resonant stimulated x-ray Raman spectroscopy of mixed-valence manganese complexes," J. Phys. Chem. Lett. **12**, 5925–5931 (2021).
[79]C. M. Loe, C. Liekhus-Schmaltz, N. Govind, and M. Khalil, "Spectral signatures of ultrafast excited-state intramolecular proton transfer from computational multi-edge transient x-ray absorption spectroscopy," J. Phys. Chem. Lett. **12**, 9840–9847 (2021).
[80]S. Biswas and L. R. Baker, "Extreme ultraviolet reflection–absorption spectroscopy: Probing dynamics at surfaces from a molecular perspective," Acc. Chem. Res. **55**, 893–903 (2022).
[81]D. Mayer, F. Lever, D. Picconi, J. Metje, S. Alisauskas, F. Calegari, S. Düsterer, C. Ehlert, R. Feifel, M. Niebuhr, B. Manschwetus, M. Kuhlmann, T. Mazza, M. S. Robinson, R. J. Squibb, A. Trabattoni, M. Wallner, P. Saalfrank, and T. J. A. Wolf, M. Gühr, "Following excited-state chemical shifts in molecular ultrafast x-ray photoelectron spectroscopy," Nat. Commun. **13**, 198 (2022).
[82]A. T. B. Gilbert, N. A. Besley, and P. M. W. Gill, "Self-consistent field calculations of excited states using the maximum overlap method (MOM)," J. Phys. Chem. A **112**, 13164–13171 (2008).
[83]G. M. J. Barca, A. T. B. Gilbert, and P. M. W. Gill, "Simple models for difficult electronic excitations," J. Chem. Theory Comput. **14**, 1501–1509 (2018).
[84]J. F. Janak, "Proof that $\partial E/\partial n_i = \epsilon_i$ in density-functional theory," Phys. Rev. B **18**, 7165–7168 (1978).
[85]K. Hui and J.-D. Chai, "SCAN-based hybrid and double-hybrid density functionals from models without fitted parameters," J. Chem. Phys. **144**, 044114 (2016).
[86]A. D. Becke, "Density-functional thermochemistry. III. The role of exact exchange," J. Chem. Phys. **98**, 5648–5652 (1993).
[87]C. Lee, W. Yang, and R. G. Parr, "Development of the Colle–Salvetti correlation-energy formula into a functional of the electron density," Phys. Rev. B **37**, 785–789 (1988).
[88]N. Mardirossian and M. Head-Gordon, "ωB97X-V: A 10-parameter, range-separated hybrid, generalized gradient approximation density functional with nonlocal correlation, designed by a survival-of-the-fittest strategy," Phys. Chem. Chem. Phys. **16**, 9904–9924 (2014).
[89]B. Alam, A. F. Morrison, and J. M. Herbert, "Charge separation and charge transfer in the low-lying excited states of pentacene," J. Phys. Chem. C **124**, 24653–24666 (2020).
[90]M. A. Rohrdanz, K. M. Martins, and J. M. Herbert, "A long-range-corrected density functional that performs well for both ground-state properties and time-dependent density functional theory excitation energies, including charge-transfer excited states," J. Chem. Phys. **130**, 054112 (2009).
[91]R. M. Richard and J. M. Herbert, "Time-dependent density-functional description of the ^1L_a state in polycyclic aromatic hydrocarbons: Charge-transfer character in disguise?," J. Chem. Theory Comput. **7**, 1296–1306 (2011).
[92]N. A. Besley, M. J. G. Peach, and D. J. Tozer, "Time-dependent density functional theory calculations of near-edge x-ray absorption fine structure with short-range corrected functionals," Phys. Chem. Chem. Phys. **11**, 10350–10358 (2009).
[93]N. A. Besley and F. A. Asmuruf, "Time-dependent density functional theory calculations of the spectroscopy of core electrons," Phys. Chem. Chem. Phys. **12**, 12024–12039 (2010).
[94]M. A. Rohrdanz and J. M. Herbert, "Simultaneous benchmarking of ground- and excited-state properties with long-range-corrected density functional theory," J. Chem. Phys. **129**, 034107 (2008).
[95]A. W. Lange and J. M. Herbert, "Both intra- and interstrand charge-transfer excited states in B-DNA are present at energies comparable to, or just above, the $^1\pi\pi^*$ excitonic bright states," J. Am. Chem. Soc. **131**, 3913–3922 (2009).
[96]M. W. D. Hanson-Heine, M. W. George, and N. A. Besley, "Basis sets for the calculation of core-electron binding energies," Chem. Phys. Lett. **699**, 279–285 (2018).
[97]J. Qian, E. J. Crumlin, and D. Prendergast, "Efficient basis sets for core-excited states motivated by Slater's rules," Phys. Chem. Chem. Phys. **24**, 2243–2250 (2022).
[98]F. Jensen, "Method calibration or data fitting?," J. Chem. Theory Comput. **14**, 4651–4661 (2018).
[99]P. M. W. Gill, B. G. Johnson, and J. A. Pople, "A standard grid for density-functional calculations," Chem. Phys. Lett. **209**, 506–512 (1993).
[100]S. Dasgupta and J. M. Herbert, "Standard grids for high-precision integration of modern density functionals: SG-2 and SG-3," J. Comput. Chem. **38**, 869–882 (2017).
[101]E. Epifanovsky, A. T. B. Gilbert, X. Feng, J. Lee, Y. Mao, N. Mardirossian, P. Pokhilko, A. F. White, M. P. Coons, A. L. Dempwolff, Z. Gan, D. Hait, P. R. Horn, L. D. Jacobson, I. Kaliman, J. Kussmann, A. W. Lange, K. U. Lao, D. S. Levine, J. Liu, S. C. McKenzie, A. F. Morrison, K. D. Nanda, F. Plasser, D. R. Rehn, M. L. Vidal, Z.-Q. You, Y. Zhu, B. Alam, B. J. Albrecht, A. Aldossary, E. Alguire, J. H. Andersen, V. Athavale, D. Barton, K. Begam, A. Behn, N. Bellonzi, Y. A. Bernard, E. J. Berquist, H. G. A. Burton, A. Carreras, K. Carter-Fenk, R. Chakraborty, A. D. Chien, K. D. Closser, V. Cofer-Shabica, S. Dasgupta, M. de Wergifosse, J. Deng, M. Diedenhofen, H. Do, S. Ehlert, P.-T. Fang, S. Fatehi, Q. Feng, T. Friedhoff, J. Gayvert, Q. Ge, G. Gidofalvi, M. Goldey, J. Gomes, C. E. González-Espinoza, S. Gulania, A. O. Gunina, M. W. D. Hanson-Heine, P. H. P. Harbach, A. Hauser, M. F. Herbst, M. Hernández Vera, M. Hodecker, Z. C. Holden, S. Houck, X. Huang, K. Hui, B. C. Huynh, M. Ivanov, Á. Jász, H. Ji, H. Jiang, B. Kaduk, S. Kähler, K. Khistyaev, J. Kim, G. Kis, P. Klunzinger, Z. Koczor-Benda, J. H. Koh, D. Kosenkov, L. Koulias, T. Kowalczyk, C. M. Krauter, K. Kue, A. Kunitsa, T. Kus, I. Ladjánszki, A. Landau, K. V. Lawler, D. Lefrancois, S. Lehtola, R. R. Li, Y.-P. Li, J. Liang, M. Liebenthal, H.-H. Lin, Y.-S. Lin, F. Liu, K.-Y. Liu, M. Loipersberger, A. Luenser, A. Manjanath, P. Manohar, E. Mansoor, S. F. Manzer, S.-P. Mao, A. V. Marenich, T. Markovich, S. Mason, S. A. Maurer, P. F. McLaughlin, M. F. S. J. Menger, J.-M. Mewes, S. A. Mewes, P. Morgante, J. W. Mullinax, K. J. Oosterbaan, G. Paran, A. C. Paul, S. K. Paul, F. Pavošević, Z. Pei, S. Prager, E. I. Proynov, Á. Rák, E. Ramos-Cordoba, B. Rana, A. E. Rask, A. Rettig, R. M. Richard, F. Rob, E. Rossomme, T. Scheele, M. Scheurer, M. Schneider, N. Sergueev, S. M. Sharada, W. Skomorowski, D. W. Small, C. J. Stein, Y.-C. Su, E. J. Sundstrom, Z. Tao, J. Thirman, G. J. Tornai, T. Tsuchimochi, N. M. Tubman, S. P. Veccham, O. Vydrov, J. Wenzel, J. Witte, A. Yamada, K. Yao, S. Yeganeh, S. R. Yost, A. Zech, I. Y. Zhang, X. Zhang, Y. Zhang, D. Zuev, A. Aspuru-Guzik, A. T. Bell, N. A. Besley, K. B. Bravaya, B. R. Brooks, D. Casanova, J.-D. Chai, S. Coriani, C. J. Cramer, G. Cserey, A. E. DePrince III, R. A. DiStasio, Jr., A. Dreuw, B. D. Dunietz, T. R. Furlani, W. A. Goddard III, S. Hammes-Schiffer, T. Head-Gordon, W. J. Hehre, C.-P. Hsu, T.-C. Jagau, Y. Jung, A. Klamt, J. Kong, D. S. Lambrecht, W. Liang, N. J. Mayhall, C. W. McCurdy, J. B. Neaton, C. Ochsenfeld, J. A. Parkhill, R. Peverati, V. A. Rassolov, Y. Shao, L. V. Slipchenko, T. Stauch, R. P. Steele, J. E. Subotnik, A. J. W. Thom, A. Tkatchenko, D. G. Truhlar, T. Van Voorhis, T. A. Wesolowski, K. B. Whaley, H. L. Woodcock III, P. M. Zimmerman, S. Faraji, P. M. W. Gill, M. Head-Gordon, J. M. Herbert, and A. I. Krylov, "Software for the frontiers of quantum chemistry: An overview of developments in the Q-Chem 5 package," J. Chem. Phys. **155**, 084801 (2021).
[102]O. Takahashi, "Relativistic corrections for single- and double-core excitations at the K- and L-edges from Li to Kr," Comput. Theor. Chem. **1102**, 80–86 (2017).
[103]L. Keller, V. Blum, P. Rinke, and D. Golze, "Relativistic correction scheme for core-level binding energies from *GW*," J. Chem. Phys. **153**, 114110 (2020).
[104]J. E. Subotnik, Y. Shao, W. Liang, and M. Head-Gordon, "An efficient method for calculating maxima of homogeneous functions of orthogonal matrices: Applications to localized occupied orbitals," J. Chem. Phys. **121**, 9220–9229 (2004).
[105]O. Travnikova, K. J. Børve, M. Patanen, J. Söderström, C. Miron, L. J. Sæthre, N. Mårtensson, and S. Svensson, "The ESCA molecule—Historical remarks and a new results," J. Electron Spectrosc. **185**, 191–197 (2012).

[106]D. Mejia-Rodriguez, A. Kunitsa, E. Aprà, and N. Govind, "Scalable molecular GW calculations: Valence and core spectra," J. Chem. Theory Comput. **17**, 7504–7517 (2021).
[107]U. Gelius, E. Basilier, S. Svensson, T. Bergmark, and K. Siegbahn, "A high resolution ESCA instrument with x-ray monochromator for gases and solids," J. Electron Spectrosc. **2**, 405–434 (1973).
[108]F. A. Delesma, M. Van den Bossche, H. Grönbeck, P. Calaminici, A. M. Köster, and L. G. M. Pettersson, "A chemical view on x-ray photoelectron spectroscopy: The ESCA molecule and surface-to-bulk XPS shifts," ChemPhysChem **19**, 169–174 (2018).
[109]S. L. Sorensen, X. Zheng, S. H. Southworth, M. Patanen, E. Kokkonen, B. Oostenrijk, O. Travnikova, T. Marchenko, M. Simon, C. Bostedt, G. Doumy, L. Cheng, and L. Young, "From synchrotrons for XFELs: The soft x-ray near-edge spectrum of the ESCA molecule," J. Phys. B: At. Mol. Opt. Phys. **53**, 244011 (2020).
[110]A. P. Bartók and J. R. Yates, "Regularized SCAN functional," J. Chem. Phys. **150**, 161101 (2019).
[111]J. W. Furness, A. D. Kaplan, J. Ning, J. P. Perdew, and J. Sun, "Accurate and numerically efficient r^2SCAN meta-generalized gradient approximation," J. Phys. Chem. Lett. **11**, 8208–8215 (2020).
[112]G. Santra and J. M. L. Martin, "Pure and hybrid SCAN, rSCAN, and r^2SCAN: Which one is preferred in KS- and HF-DFT calculations, and how does D4 dispersion correction affect this ranking?," Molecules **27**, 141 (2022).
[113]O. Plekan, V. Feyer, R. Richter, M. Coreno, M. de Simone, K. C. Prince, A. B. Trofimov, E. V. Gromov, I. L. Zaytseva, and J. Schirmer, "A theoretical and experimental study of the near edge x-ray absorption fine structure (NEXAFS) and x-ray photoelectron spectra (XPS) of nucleobases: Thymine and adenine," Chem. Phys. **347**, 360–375 (2008).
[114]J. D. Wadey and N. A. Besley, "Quantum chemical calculations of x-ray emission spectroscopy," J. Chem. Theory Comput. **10**, 4557–4564 (2014).
[115]Y. Zhang, S. Mukamel, M. Khalil, and N. Govind, "Simulating valence-to-core x-ray emission spectroscopy of transition metal complexes with time-dependent density functional theory," J. Chem. Theory Comput. **11**, 5804–5809 (2015).
[116]I. P. E. Roper and N. A. Besley, "The effect of basis set and exchange-correlation functional on the time-dependent density functional theory calculations within the Tamm–Dancoff approximation of the x-ray emission spectroscopy of transition metal complexes," J. Chem. Phys. **144**, 114104 (2016).
[117]C. J. Clarke, S. Hayama, A. Hawes, J. P. Hallett, T. W. Chamberlain, K. R. J. Lovelock, and N. A. Besley, "Zinc 1s valence-to-core x-ray emission spectroscopy of halozincate complexes," J. Phys. Chem. A **123**, 9552–9559 (2019).
[118]Y. Zhang, U. Bergmann, R. Schoenlein, M. Khalil, and N. Govind, "Double core hole valence-to-core x-ray emission spectroscopy: A theoretical exploration using time-dependent density functional theory," J. Chem. Phys. **151**, 144114 (2019).
[119]T. Fransson and A. Dreuw, "Simulating x-ray emission spectroscopy with algebraic diagrammatic construction schemes for the polarization propagator," J. Chem. Theory Comput. **15**, 546–556 (2019).
[120]D. R. Nascimento and N. Govind, "Computational approaches for XANES, VtC-XES, and RIXS using linear-response time-dependent density functional theory based methods," Phys. Chem. Chem. Phys. **24**, 14680–14691 (2022).
[121]T. J. Penfold and C. D. Rankine, "A deep neural network for valence-to-core x-ray emission spectroscopy," Mol. Phys. e2123406 (published online).
[122]M. Annegarn, J. M. Kahk, and J. Lischner, "Combining time-dependent density functional theory and the ΔSCF approach for accurate core-electron spectra," J. Chem. Theory Comput. **18**, 76220–77629 (2022).
[123]See http://osc.edu/ark:/19495/f5s1ph73 for more information about Ohio Supercomputer Center.